Performance of Conducting Polyaniline-DBSA and Polyaniline-DBSA/Fe_3O_4 Composites as Electrode Materials for Aqueous Redox Supercapacitors

S. Radhakrishnan, Chepuri R. K. Rao,* M. Vijayan

Functional Materials Division, Central Electrochemical Research Institute, Karaikudi-630006, India

Received 13 September 2010; accepted 25 January 2011
DOI 10.1002/app.34236
Published online 26 May 2011 in Wiley Online Library (wileyonlinelibrary.com).

ABSTRACT: This article reports the synthesis, characterization and supercapacitative properties of dodecyl benzenesulphonic acid (DBSA) doped polyaniline(PAni) and its magnetite composites. The synthesized composites are characterized by Uv-Vis, FT-IR, XRD, SEM, electrochemical methods and are evaluated as electrode material for supercapacitor applications. The composites are partially soluble in methanol and are highly dispersible in water. The pristine polyaniline (PAni-DBSA) showed a specific capacitance of 160 F/g, whereas its magnetite(3.8 wt %) composite (C1) and the symmetrical capacitor derived from C1 showed enhanced capacitance of 228 F/g and 180 F/g respectively, at 1 mA/cm^2. © 2011 Wiley Periodicals, Inc. J Appl Polym Sci 122: 1510–1518, 2011

Key words: polyaniline; magnetite; supercapacitor; charge-discharge; current density

INTRODUCTION

Conducting polymers (CPs) now own a special status in the field of electroactive materials especially after the pioneering and noble prize winning contributions by Shirakawa-McDiarmid-Heeger group in the year 2000.[1] After this, a great deal of progress has been made on these synthetic metals in terms of their synthesis, processability and device applications.[2–4] Particular attention has been given on polyaniline (PAni) due to its stability, thin film-forming property with tunable conductivity due to controlled acid-base doping and most importantly due to its commercial viability. Polyanilines have been studied extensively due to their applications to practical devices for energy storage, electrochemical sensors, electrochromic devices, electromagnetic interference (EMI) shielding, and corrosion protection.[3–10] Application of the CPs in energy storage devices is also well known[11] and recent studies[12–15] in this area gave impetus to fundamental and applied research on CP-based new materials.

Supercapacitors are energy storage devices which can be fabricated with high power and high energy density and possibly bridge the gap between high power density capacitors and high energy density batteries.[16] When incorporated into a battery-based power source, it adds to the capability for meeting the burst power demands in applications such as electric vehicles.[17,18] Basically there are three categories of materials which are used as supercapacitor electrode materials (i) carbons, (ii) metal oxides, and (iii) conducting polymers. Double layer capacitance is major contribution for capacitance in the first type of materials whereas redox reactions are responsible for the major contribution for the capacitance (known pseudo capacitance) in the latter two types of materials. Transition metal oxides are promising materials for supercapacitor application, for example RuO_2, IrO_2,[19–22] but these are not preferred due to their high cost. Other oxides such as Fe_3O_4,NiO_x, Co_3O_4, V_2O_5, and MnO_2 are also known for the use of supercapacitor materials.[23–26] Conducting polymers, namely, polyaniline, polypyrrole, and polythiophene, are the next best opted materials for this purpose as they exhibit as high as 500 C/g charge capacity.[27–30] CPs are promising materials for supercapacitors[14] for the reasons that (i) these exhibit high specific capacitance as the redox process occur in entire polymer mass and (ii) these exhibit high conductivity in the charged state so that the device with low ESR can be possible which is vital in deciding maximum usable power. Moreover CPs are flexible and are also low density materials compared with metal oxides and hence favor easy fabrication of low weight and flexible devices.

**Present address:* Organic Coatings and Polymers Division, Indian Institute of Chemical Technology (IICT), Hyderabad-500007.

Correspondence to: C. R. K. Rao (ramchepuri@gmail.com).

Earlier, we reported the synthesis and bifunctional utility of organically soluble polyaniline-magnetite composites which can be useful in sensing dopamine and as supercapacitor material.[31] The composite material on stainless steel (S.S) as current collector exhibited a specific capacitance as high as 213 F/g. This article studies, in detail, the supercapacitative properties of the polyaniline-magnetite composites with various loadings of magnetite in polyaniline. The composites are synthesized and characterized by formal spectral methods and are evaluated as electrode material for supercapacitor applications. The results are presented and discussed.

EXPERIMENTAL

Materials and methods

Analytical grade aniline monomer was purchased from Merck, India. Stainless steel foil (0.05 mm, Type 304) was purchased from AlfaAesar and contained Fe:Cr:Ni in 70 : 19 : 11 wt %. Dodecylbenzene sulfonic acid (70 wt % solution in 2-propanol) (DBSA) was purchased from Aldrich chemical company. X-ray diffraction patterns (XRD) were obtained with PANalytical MPD diffractometer using Cu K_α radiation. FT-IR spectra of KBr powder-pressed pellets were recorded on model no.nexus-670 spectrometer from Thermonicolet. spectrometer. Conductivity of the samples were measured by four-probe method using KEITHLEY nanovoltmeter after pressing the samples into 1 cm dia, 1.5 mm thick pellets under 3 ton pressure. Cyclic voltammetry was performed on AUTOLAB 302 electrochemical system using three electrode assembly consisting of a platinum foil (2 mm x 2.5 mm) working electrode, a glassy carbon rod (2 mm diameter, 8 cm long) as auxiliary electrode and a S.C.E as reference electrode. Solartron Electrochemical analyzer (Model 1287) was used for Impedance spectra. Charge-discharge experiments were also conducted on AUTOLAB 302 electrochemical system using a fabricated S.S composite electrode.

Synthesis of PAni-DBSA -Fe_3O_4 nanocomposites

Fe_3O_4 magnetic particles were prepared by precipitation-oxidation method according to a known procedure.[32] PAni-magnetite composites were prepared by an in situ polymerization of aniline (1 mL) in DBSA (10 mL in 100 mL water) solution containing specific amount of Fe_3O_4 magnetic particles according to the known procedure.[33] The main difference in the present synthesis is low loading of Fe_3O_4 material ranging from 0.1 g, 0.2 g, and 0.3 g per 1 mL of aniline and using acid form of DBSA instead of salt form (Na-DBSA) in the known procedure. A typical procedure for composite C1 is given below.

Magnetite particles (0.1 g) were mixed into 90 mL water containg 10 mL of DBSA (Aldrich,70 wt % in 2-propanol) and were sonicated for 30 min for effective dispersion. To this was added 1 mL of aniline (10.7 m*M*) and stirred vigorously for 1 h. Ammonium persulphate (APS, 2.28 g, 10 m*M*)) in 25 mL of water, was added to the above solution dropwise and stirring continued for 12h. The dark green resulting precipitates were filtered through no.42 filter paper and washed thoroughly with water until filtrate is colorless and finally dried in oven at 50°C. The polymerized products are designated as C-1, C-2, and C-3 for Fe_3O_4 loadings of 0.1, 0.2, and 0.3 g, respectively. The weight% of the magnetite was calculated from the yield of the composite obtained and were rechecked with CHNS elemental analyses which were found to be as 3.55, 7.49, and 11.19 wt %, respectively. A control sample (PAni-DBSA) was also prepared without addition of Fe_3O_4 particles and studied along with the composites for comparison.

Electrode preparation

The composite electrodes with S.S as current collectors (1 cm^2) were prepared using polyvinylidene fluoride (PVDF, 10 mg, Fluka) as binder, activated carbon (10 mg, Fluka) as diluter and conductor and the composite C1(or C2 or C3) (80 mg). First PVDF was dissolved in *N*-methylpyrrolidone (NMP) solvent and other ingredients were thoroughly mixed into it by manual grinding in a mortar. The resulting slurry was uniformly coated on the S.S electrode and dried at 50°C for 24 h. The two electrodes were tightly placed together with a fresh cotton cloth as separator and tied with nylon tag. This symmetrical capacitor was subjected to charge-discharge tests from 0.0 to 0.75 V in 1*M* sulfuric acid and the specific capacitance(SC), specific power (SP), and specific energy (SE) values were calculated from discharge times[29,34] by the following relationships:

$$\text{S.C(F/g)} = I(A) \times t(s)/\Delta E \times m$$
$$\text{SP (W/kg)} = I(A) \times \Delta E/m$$
$$\text{SE (Wh/kg)} = I(A) \times t(s) \times \Delta E/m$$

where I = current (A), t = discharge time (s), m = mass of the electroactive material on two electrodes and ΔE is the potential window scanned.

RESULTS AND DISCUSSION

Formation, composition, and characterization of the composites

In addition to its strong proton donating ability, which is needed for PAni for inducing conductivity,

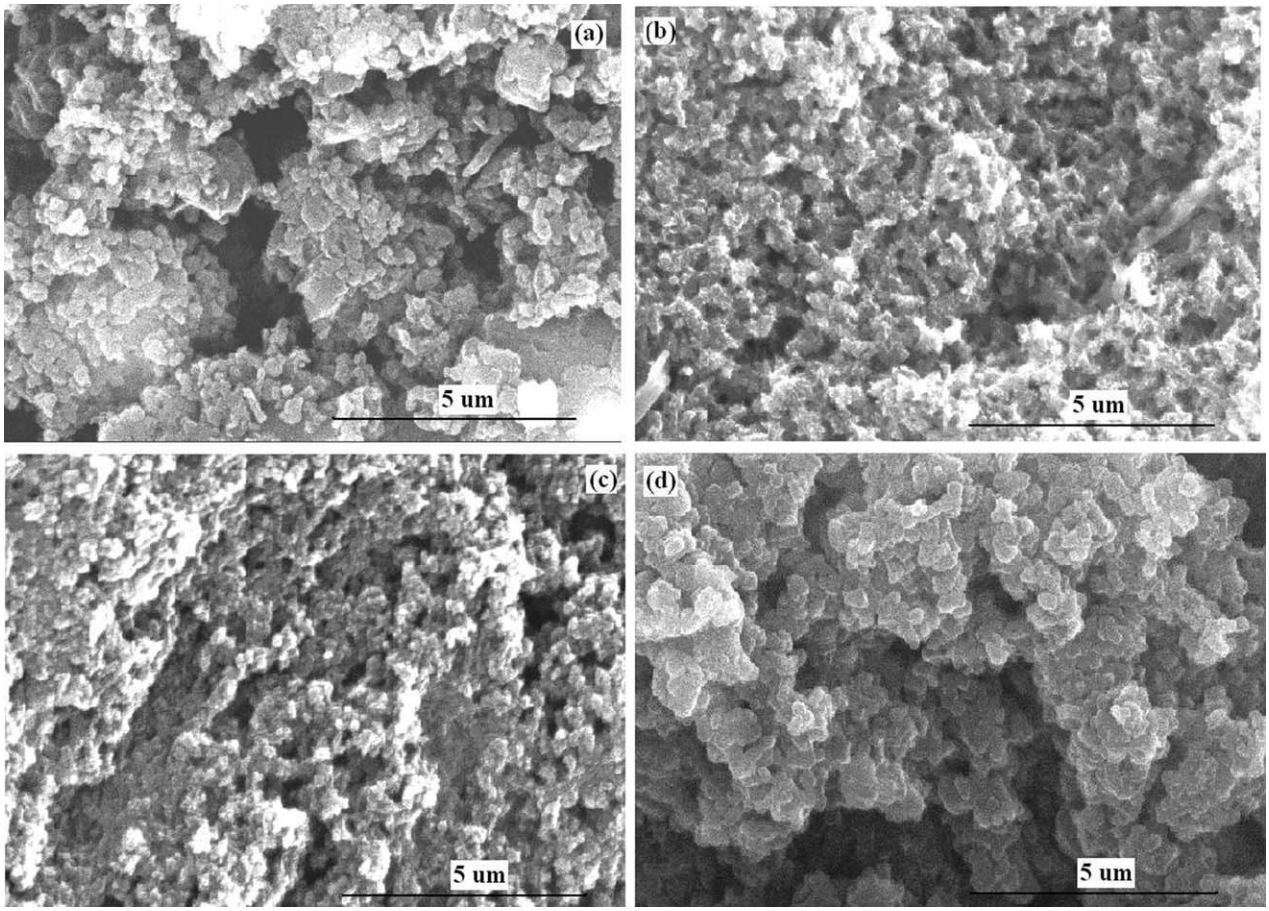

Figure 1 Scanning electron micrograph of a) pure Pani-DBSA b) composites C1 c) Composite C2 and d) composite C3

the presence of long chain in DBSA makes it as a good surfactant. Because of this reason, the prepared composites C-1, C-2, and C-3 are partially soluble in chloroform, methanol and dispersible in water. However, the solubility/dispersibility decreases with increase in oxide incorporation, i.e., the order C1>C2>C3 is noticed. Dramatic effect in particle size and morphology is observed for the composites when magnetite is added into polyaniline. The size of the particles (50–100 μm) in the pristine polymer is greatly reduced to about 0.5–1 μm for the composites (Fig. 1). This is due to the smaller size of magnetite particles (30 nm) which acted as nulclei for the formation of PAni particles. As the concentration of the magnetite increased the particle size also increased, as seen from the SEM profiles in Figure 2. Thus it is expected that the composite C1 has maximum surface area compared with the pure polymer or C2 and C3 and hence also expected to exhibit higher capacitance values, which indeed observed. We could not perform the TEM analysis of these composites to evaluate the size and morphology due to magnetic nature. On the basis of the data from C, H, N, and S elemental analyses collected in Table I, Polyaniline-magnetite composites are formed with magnetite loadings of 3.55, 7.49, and 11.19 wt %.

The characteristic FT-IR peaks (Table I) of conducting PAni-DBSA, attributable to C=C stretching of benzenoid (*N*—B—N) and quinoid (N=Q=N) segments in the polymer chain are observed at 1558

TABLE I
Composition, Conductivity, and Spectral Data of the Samples

Polymers/ composites	FT-IR (KBr pellet)(cm^{-1})				Conductivity (S/cm)	C%, H%, N%, S% (respectively for EB.1DBSA.xFe_3O_4)	Oxide content (wt%)
	$C\text{-}N_{(ar)}$	N-B-N	N-Q-N	N-H			
PAni-dbsa	1295	1470	1558	3436	0.502	73.25, 6.97, 8.13, 6.90	0.0%
C1	1296	1474	1562	3434	0.551	70.46, 6.71, 7.82, 4.47	3.55%
C2	1295	1469	1557	3430	0.571	67.28, 6.44, 7.51, 4.29	7.49%
C3	1296	1461	1559	3429	0.597	64.89, 6.18,7.20, 4.12	11.19%

and 1470 cm^{-1}. The peak observed at 1296 cm^{-1} is assigned to the C—N stretching vibration of the benzenoid ring. The band fell in the range 879 cm^{-1} is identified as the out-of-plane bending of C—H bond in the 1,4-disubstitued ring. The peak at about 1115 cm^{-1} is related to the poloron band formed by doping. The $R\text{-}SO_3^{-1}$ group of doped DBSA is seen at 1037 cm^{-1}. The C—H_{ar} stretching is observed at 2922 cm^{-1}[35]. The composites also exhibit very similar IR bands. The main difference between iron oxide composites and pure PAni-DBSA is the decrease of NH- stretching band intensity in former cases which is possibly due to -HN...Fe_3O_4 interaction in the composites. The UV-Vis spectrum (Fig. 2) of C1 in basic NMP solvent exhibited bands at 321 nm, 420 nm and 601 nm suggesting that PAni is partially doped state. The fully doped state for the polymer is achieved by addition of few drops of HCl to this solution. This results in the electronic bands to appear at 350 nm [assignable to $\pi \rightarrow \pi^*$ of benzenoid structures], 427 nm [excitations to polaron band] and 805 nm [excitations to polaron band].[35–37]

XRD studies on the composites revealed the inclusion of Fe_3O_4 particles in the composites (Fig. 3). The profile exhibited peaks assignable to reflections due to (220), (311), (400), (422), (511), (440) at 2θ = 30.16, 35.49, 43. 12, 53.55, 57.05, and 62.64 respectively, due to Fe_3O_4 particles.[38] PAni matrix is amorphous and showed broad hump centered at 2θ = 20 and a relatively sharper but still broad peak at 2θ = 25.31. The former peak is ascribed to periodicity parallel to the polymer chain and the latter peak may be caused by the periodicity perpendicular to the polymer chain.[39] The intensity of the peaks due to iron oxide increases upon increase of its loading in the composite from C1 to C3. The pristine polymer showed a conductivity of 0.5 S/cm (Table I). The composites C1-C3 showed slightly higher conductivity of 0.551, 0.571, and 0.597 S/cm respectively, due to the presence of magnetite particles.

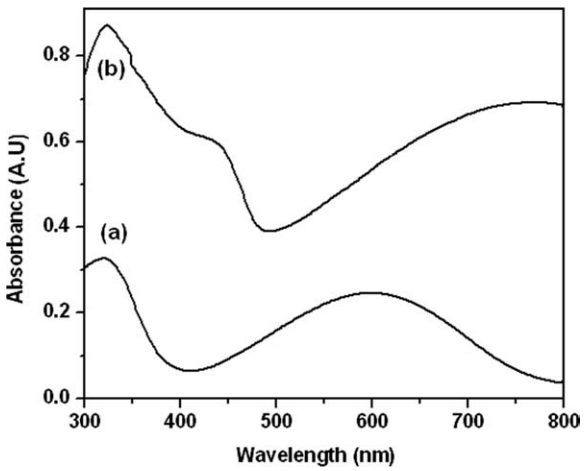

Figure 2 Uv-Vis spectrum of C1 in NMP solvent a) as prepared b) after addition of few drops of con.HCl

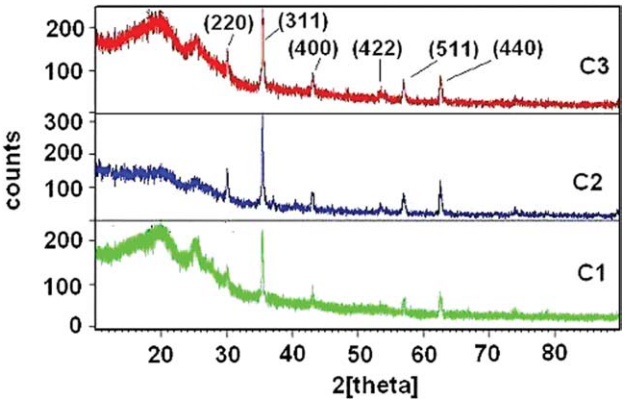

Figure 3 XRD profiles of the composites. [Color figure can be viewed in the online issue, which is available at wileyonlinelibrary.com.]

Electrochemical activity of the composites has been investigated. Figure 4A(b) shows the cyclic voltammogram of the composite on Pt foil electrode in 1*M* sulfuric acid. Two anodic oxidations of PAni take place at 0.288 V, 0.784 V, and reductions at 0.651V and 0.10 V suggesting the presence of conducting PAni. A middle oxidation peak generally observable for pure PAni at about 0.4 V assignable to benzoquinone impurities/degradation products is seen with low intensity and suggests that the impurities are present in lower amounts. The plot of $v^{1/2}$ versus anodic peak current is linear and hence the electron transfer is diffusion controlled. Pristine polymer PAni-DBSA [Fig. 4(A), a] showed the oxidation peaks at 0.186 V and 0.684 V which are nearly 100 mV less than composite C1. This suggests that electron transfers are more facile in the pristine than in composite C1. The parallelogram shape for the CV with high current suggests that the material is useful for supercapacitor application.

Capacitance of single electrodes

Very few reports are available on the use of Fe_3O_4 (or its composites) for supercapacitor applications.[40,41] Pure Fe_3O_4 material[40] showed a specific capacitance of 5–7 F/g where as dispersion of this material on carbon black lead to high specific capacitance in the range 30–510 F/g. Barring our earlier communication,[31] to the best of our knowledge, there is no report on the use of this material composited with PAni for the use of supercapacitor. Hence, the pristine polymer and composites C1-C3 were tested for their supercapacitance properties.

Single electrodes were subjected for charge-discharge tests at different current densities. Figure 5 shows the charge-discharge cycling curves for the

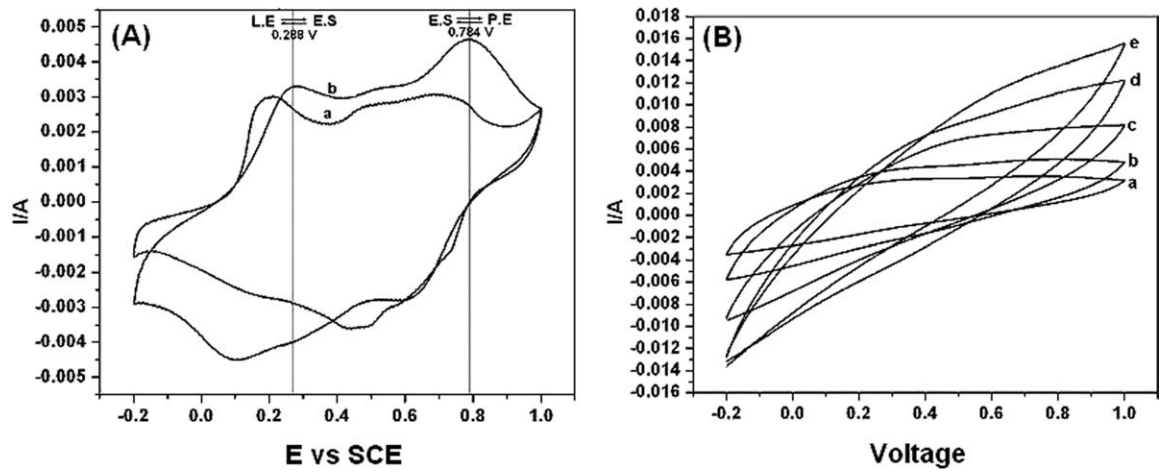

Figure 4 A: Cyclic voltammogram (CV) of pristine polymer (a) PAni-DBSA and (b) composite C1 on Pt electrode recorded at 100mV/s in 1*M* sulfuric acid. The figure also shows the transition potentials for LE ↔ES ↔ PE states for the composite (B) CV of fabricated supercapcitor at the scan rates of 100 to 500 mV/s (a–e).

C1-C3 composite electrodes at a current density of 3 mA/cm^2. Table II lists specific capacitance of the single electrodes at different current densities. Composite with lowest incorporation of magnetite (C1) showed highest SC value of 228 F/g at 1 mA/cm^2. This value decreases to 180 F/g at 5 mA/cm^2. The SC values decrease to 176,173 F/g for the composites C2 and C3 at this 1 mA/cm^2 current density. These values further decrease to 143 F/g and 130 F/g for 5 mA/cm^2 current density. The stability of the composite electrodes against 1000 charge-discharge cycles was tested [Fig. 5(d)] at current density of

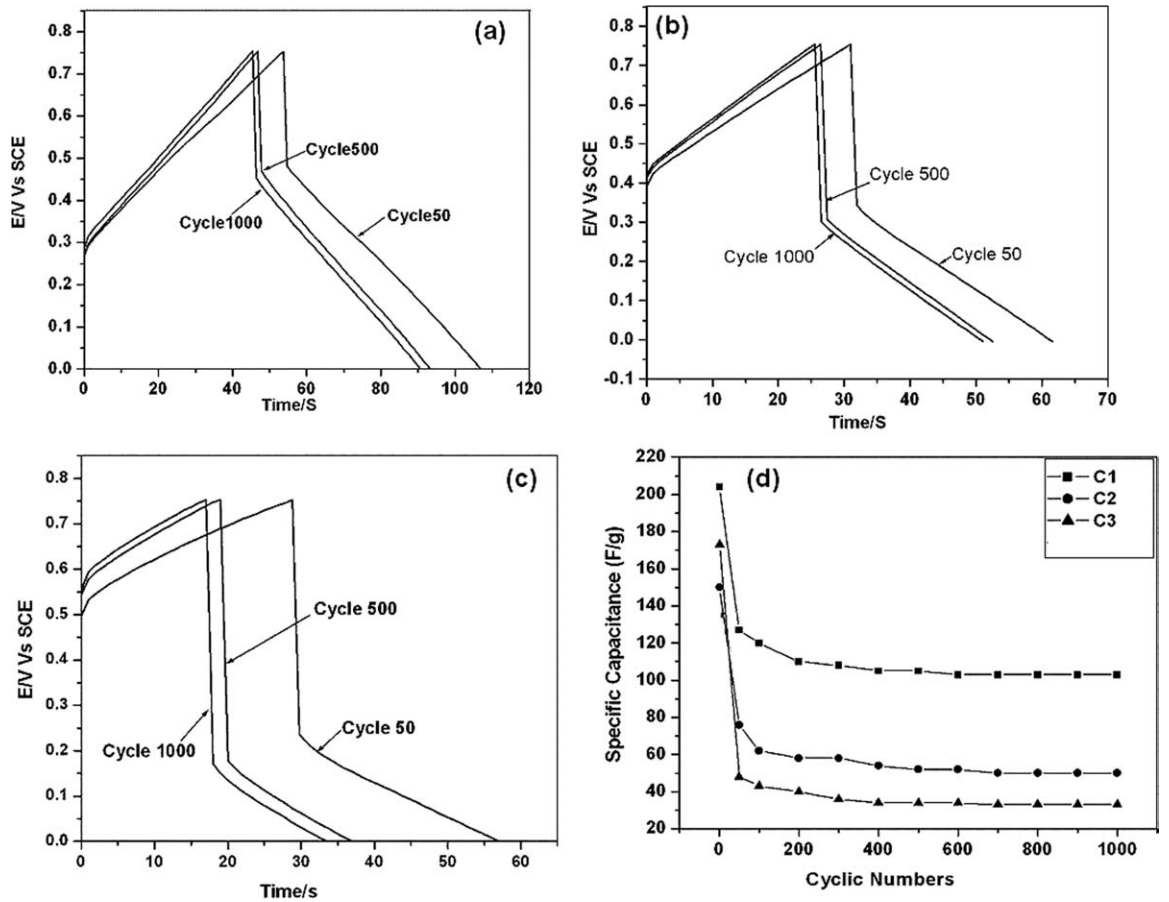

Figure 5 Charge-discharge curves for the single electrodes (a) C1 (b) C2 (c) C3 at C.D = 3 mA/cm^2 and (d) graph showing specific capacitance of the above electrodes with cycle number.

TABLE II
Capacitance Data of the Composites and Capacitor at Different Current Densities and Cycle Numbers

	Specific capacitance (F/g)				
Composite electrodes	@1mA/cm^2 Ist cycle	2 mA/cm^2 Ist cycle	3 mA/cm^2 Ist cycle (1000th cycle)	4 mA/cm^2 Ist cycle	5 mA/cm^2 Ist cycle (1000th cycle)
Pani-single electrode	160	137	117	101	86
C1-single electrode	228	216	204 (103)	194	180
C2-single electrode	176	160	150 (50)	146	143
C3-single electrode	173	154	144 (33)	140	130
C1-capacitor	180	160	156	147	135 (84)

3 mA/cm^2 and the data is collected in Table II (in parentheses). Figure 5(a–c) shows that charging and discharging times fall with cycle number. This is also reflected in specific capacitance values. The fall in charge-discharge times is more (about 48%) for first 500 cycles and is less for latter 500 cycles (about 2%). The rapid deterioration of specific capacitance values is due large internal resistance of the electrode which causes large ohmic drop at high discharge current density.[42] It is also observed from the charge-discharge curves that there is considerable resistance (ESR) while charging and discharging as evident from sharp jump in the voltage jump. The estimated ESR ($=\Delta V/I$) is about 1 Ω cm^2 when 1 mA/cm^2 current density is used.

Assembled capacitor

A symmetrical capacitor was assembled as described in experimental section and was studied for its capacitance properties. Table II lists the capacitance values evaluated from the studies. Figure 4(b) shows the CV behavior of the fabricated capacitor at various scan rates. Figure 6(a) shows the first three charge-discharge curve of the device at current density from 1 mA/cm^2. Figure 6(b) shows the charge-discharge curves for 1st, 50th, and 1000th cycles for the capacitor at a current density of 5 mA/cm^2. The capacitor exhibited a capacitance of 180–135 F/g at 1–5 mA/cm^2 (Table II). The capacitance is about 75–79% of the single electrode capacitance values. The capacitor showed a decrease in capacitance to 135 F/g at 5 mA/cm^2. The charge-discharge tests carried for 1000 cycles at this current density (5 mA/cm$^{2)}$ showed that the capacitance value falls to 84 F/g in the last charge-discharge cycle. The decrease, from the first to 1000th, is about 35% and indicates that there is a degredation of electrolytes and PAni[43] during the cycling experiments. The reduction in the capacitance per discharge cycle is only 0.035% which is 10 times smaller than reported in literature.[44] There is a sudden jump in voltage in charge-discharge curves; this suggests reasonable IR drop which is apparently decreased compared to the single electrode. Figure 6(d) shows the variation of coulombic efficiency of the capacitor with cycle number. Coulombic efficiency[45] (η) is calculated as $\eta = (t_d/t_c) \times 100$ where t_d and t_c are discharge and charge times. The value which is low at 70% for first 100 cycles rises to 97% on further cycling. The other two important electrical parameters, power density, and energy density of the capacitor has been estimated from the active masses of the two electrodes and has been shown in Figure 7. The capacitor exhibited a power density of 0.407 kW/kg with an energy density of 6.33 Wh/kg at a discharge current density of 0.44 A/g. The power density value decreased to 0.081 kW/kg with energy density of 8.37 Wh/kg at a discharge current density of 0.085 A/g.

Mechanism of charging-discharging

Polyaniline exhibits two pairs of major redox peaks encompassing three oxidation states of PAni, which involve leucoemeraldine (LE), emeraldine (ES), and pernigraniline (PE) (Fig. 2). The oxidation process involves insertion of anions into the polymer chain. In the discharged state of a capacitor, PAni of both the positive and negative electrodes is in ES form, and the capacitor voltage is close to 0 V. Upon charging of the capacitor between 0 and 0.75 V, the positive electrode transforms from ES to PE state, whereas the negative electrode transforms from ES to LE state. Therefore, half the N atoms of the PAni allow insertion of HSO_4^- ions in the positive electrode and a similar number of N atoms allow expulsion of HSO_4^- ions from the negative electrode at a given time. There is no mechanism available in literature for the oxidation (charging) step when Fe_3O_4 used as electrode material. However, there are couple of reports[24] which showed that magnetite is electroactive and useful in the potential range -0.8 to 0.5V for as supercapacitor material. Here we propose that there is preferential oxidation of Fe(II) center in Fe_2O_3.FeO to Fe(III) as shown below with intake of HSO_4^- ions into the composite which are expelled in the discharge step due to reduction of Fe(III) back to Fe(II). Thus two Faradaic oxidation

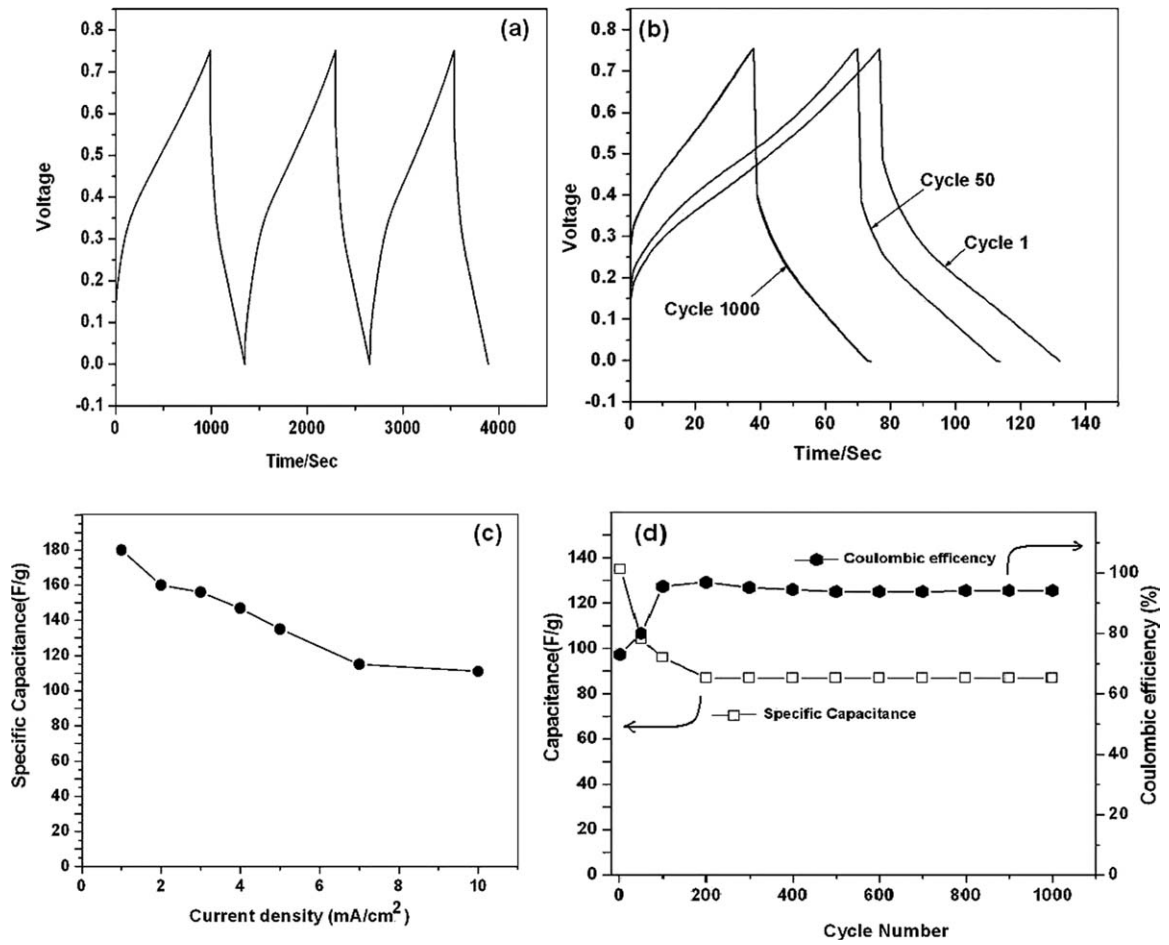

Figure 6 (a) charge-discharge curves for first three cycles exhibited by symmetric capacitor of C1 at C.D = 1 mA/cm^2 (b) Charge-discharge curves for various cycles exhibited by capacitor of C1 at C.D = 5 mA/cm^2 (c) variation of specific capacitance of the capacitor with current density (d) capacitance and columbic efficiency of the of C1 capacitor with cycle numbers.

reactions occur at one electrode surface while charging or discharging and are coupled together to enhance the specific capacitance of the composite synergistically. Thus the following mechanism should operate in the composite while charging and discharging.

Charging: PAni + $H_2SO_4 \rightarrow [PAni.H^{+\cdot}]HSO_4^-$ and
$Fe_2O_3.FeO \rightarrow Fe_2O_3.FeO^+(HSO_4^-)$
Discharging: $[PAni.H^{+\cdot}]HSO_4^- \rightarrow PAni + H^+ + HSO_4^-$
and $Fe_2O_3.FeO^+(HSO_4^-) \rightarrow Fe_2O_3.FeO + HSO_4^-$

It can be noticed that the specific capacitance of the single electrode of pure PAni- DBSA increased after the addition of magnetite particles (i.e., composite C1) which is also due to the increased surface area (due to lower particle size) apart from the contributions from reversible redox process of magnetite particles. However the S.C values decreased with increase in magnetite loadings for C2 and C3. This may be due to higher particle size

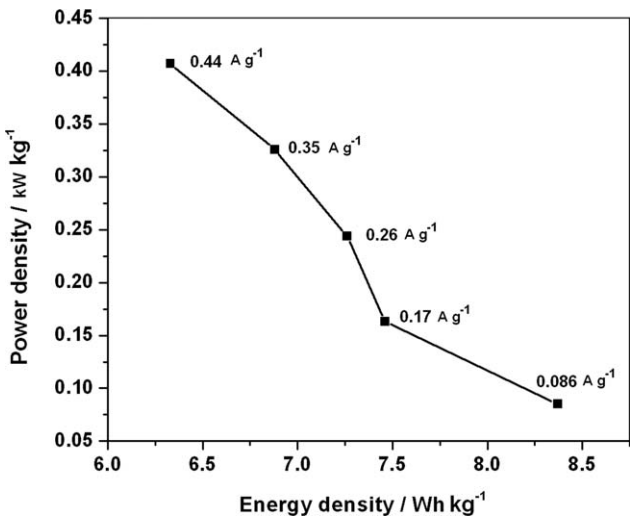

Figure 7 Plot of specific power versus specific energy of C1 symmetrical capacitor based on active mass on the electrodes.

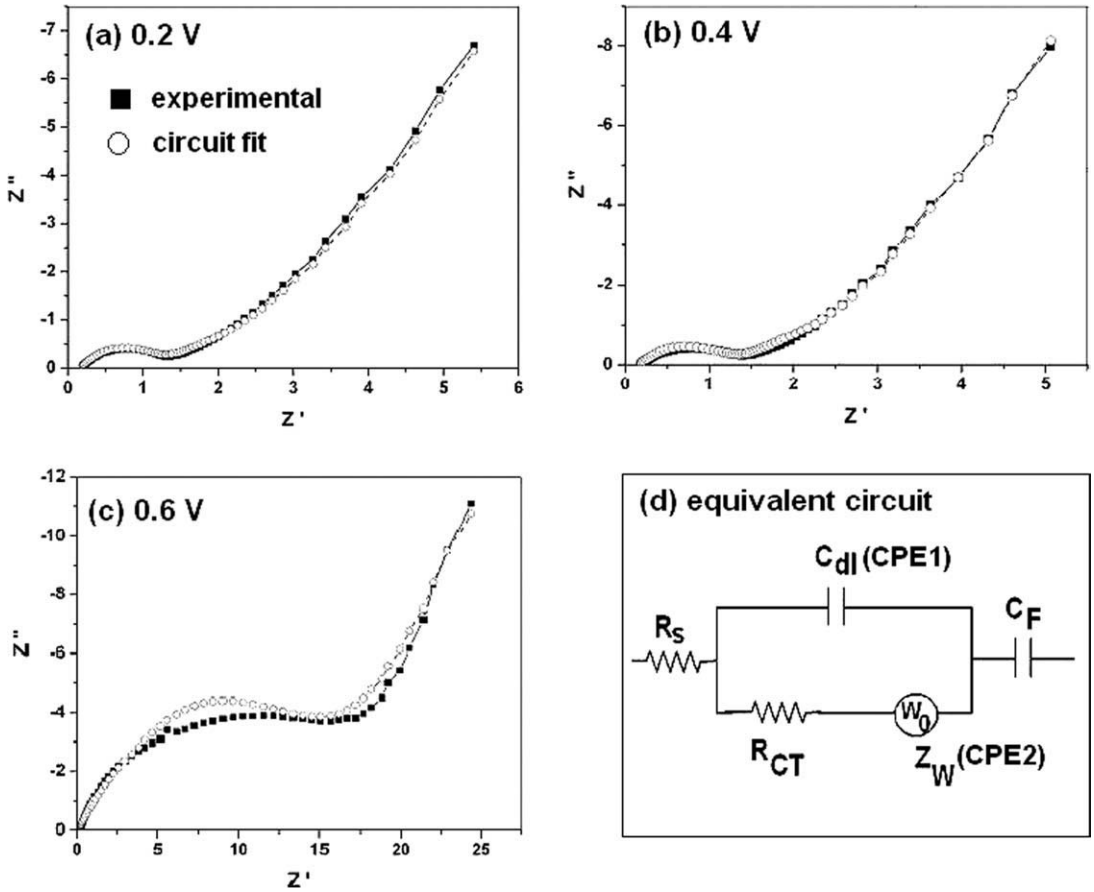

Figure 8 Nyquist plots for the capacitor C1 (a) at 0.2 V (b) at 0.4 V and (c) at 0.6 V and (d) equivalent circuit used for the system.

(lower surface area) formed with higher loadings of magnetite particles which probably offsets the increase in SC arising from redox process of magnetite particles.

Electrochemical impedance spectroscopy studies

Electrochemical impedance spectroscopy (EIS) was employed to obtain equivalent circuit parameters such as transfer resistance and ohmic resistance which enable mechanistic characterization of the system. Typical Nyquist plots for the capacitor in 1*M* sulfuric acid at potentials at 0.2, 0.4, and 0.6 V are shown in Figure 8.

The high-frequency intercept of the semicircle on the real axis provided the value of ohmic resistance (R_{sol}), and the diameter of the semicircle gave an approximate value of the charge transfer resistance (R_{ct}) of the composite/electrolyte interface. The value of R_{sol} is not much change and lie between 0.20 to 0.225 Ω for the voltages 0.2 to 0.6 V of the capacitor. But, the value of R_{ct} increased with the capacitor voltage between 0.2 and 0.6V which is evident from the increased diameter of the semicircle. It is known that the conductance of PAni is maximum between ES and PE states and it decreases when PAni transforms in to the LE state. Since the negative electrode of the capacitor gradually changes to the LE state when the voltage of the capacitor is increased, hence R_{ct} value also increased. The electrical parameters deduced from impedance plots using equivalent circuit shown in Figure 8 are collected in Table III. The estimated values of the capacitance from the EIS study are in agreement with experimental values obtained from charge-discharge curves.

TABLE III
System Parameters Obtained from Nyquist Plots

S.No	Potential (V)	R_{ct} (Ω cm^2)	CPE_1 (Ω^{-1} cm^{-2}s)	CPE_2 (Ω/S)
1	0.2	0.93 ± 0.2	0.00019 ± 0.0005	0.686
2	0.4	1.005 ± 0.2	0.00015 ± 0.0003	0.690
3	0.6	14.89 ± 1	0.0023 ± 0.0001	0.306

CONCLUDING REMARKS

Majority of the reports on super capacitor studies on polyaniline are based on electrochemically deposited

polyaniline directly on electrodes such as Pt, S.S, graphite, and carbon paper.[29,46] These electrode systems showed high specific capacitance of the order of 700–800 F/g values due to their three-dimensional nanofiber networks, porosity, thin layer formation and substrate effects. These favorable properties are effectively limited in chemically prepared polyaniline samples where the size of the particle are in the range of few micrometers. More over, chemically prepared samples are more prone for impurities than electrochemically prepared samples. Not many reports are there in literature which shows high capacitance, high power density and high energy density exhibiting chemically synthesized polyaniline or its composites.[47–51] Thus, our report is the first report that shows high capacitance, high energy and power density supercapacitor electrode material based on polyaniline-magnetite composite.

In summery, for the first time, it has been demonstrated that (i) polyaniline-magnetite composites are useful as electrode materials for supercapacitor applications (ii) the pristine polymer, PAni-DBSA, showed a lower specific capacitance of 160 F/g, whereas the single electrode of composite C1 and the symmetrical capacitor of C1 (with a 3.8 wt % loading of magnetite) showed enhanced capacitance of 228 F/g and 180 F/g at 1 mA/cm^2 respectively, (iii) the capacitance values increased with decreased loadings of magnetite particles, (iv) the composites are organically soluble and dispersible in water.

Authors sincerely thank the Director, CECRI for his encouragement and for providing new instrumental facilities.

References

1. Shirakawa, H.; Louis, L. J.; McDiarmid, A. G.; Chang, C. K.; Heeger, A.J. J Chem Soc Chem Commun 1977, 578.
2. Skotheim, T. A. Handbook of Conducting Polymers; Marcel Dekker; New York 1986; Vols. I and II.
3. Trivedi, D. C. Handbook of Organic Conductive Molecules and Polymers; Nalwa, H.S.; Eds.; Wiley, Chichester: England, 1997; Vol. 2.
4. Park, S. M. Handbook of Organic Conductive Molecules and Polymers; Nalwa, H. S.; Eds.; Wiley; Chichester, England, 1997; Vol. 3.
5. Hugot, L. G. Handbook of Organic Conductive molecules and Polymers; Nalwa, Eds.; Chichester, England: Wiley, 1997; Vol. 3.
6. Kitani, A.; Kaya, M.; Sasaki, K. J Electrochem Soc 1986, 133, 1069.
7. MacDiarmid, A. G. Synth Met 1997, 84, 27.
8. DeBerry, D. W. J Electrochem Soc 1985, 132, 1022.
9. Wang, Y.; Jing, X. Pol Adv Technol 2005, 16, 344.
10. Malinauskas, A. Synth Met 1999, 107, 75.
11. In Electrochemical Supercapacitors Scientific Fundamental and Technology Applications; Conway, B. E., Ed.; Kluwer Academic, Plenum: New York, 1999.
12. Mark, H.; George, Z.; Milo, S. P. S.; Derek, J. F.; Alan, H. Windle Chem Matter 2002, 14, 1610.
13. He, B. L.; Zhou, Y. K.; Zhou, W. J.; Dong, B.; Li, H. L. Mater Sci Eng A 2004, 374, 322.
14. Mastragostino, M.; Arbizzani, C.; Soavi, F. J Power Sour 2001, 97, 812.
15. Sun, L. J.; Liu, X. X. Eur Poly 2008, J 44, 219.
16. Kotz, R.; Carlen, M. Electrochim Acta 2000, 45, 2483.
17. Mastragostino, M.; Arbizzani, C.; Paraventi, R.; Zanelli, A. J Electrochem Soc 2002, 147, 407.
18. In Hand book of Organic Conductive Molecules and Polymers; Arbizzani, C.; Mastragostino, M.; Scrosati, Nalwa, H. S.; Eds.; Wiley: Chichester, UK, 1997; Vol. 4.
19. Trasatti, S.; Kurzweil, P. Plat Met Rev 1994, 38, 46.
20. Conway, B. E. J Electrochem Soc 1991, 138, 1539.
21. Sarangapani, S.; Tilak, B. V.; Phen, C. P. J Electrochem Soc 1996, 143, 371.
22. Ye, J. S.; Cui, H. F.; Liu, X.; Lim, T. M.; Zhang, W. D.; Sheu, F. S. Small 2005, 1, 560.
23. Srinivas, V.; Weidner, J. W. J Power Sources 2002, 108, 15.
24. Brousse, T.; Belangar, D. Electr Solid State Lett 2003, 6, A244.
25. Wang, S. Y.; Wu, N. L. J Appl Electrochem 2003, 33, 345.
26. Cottineau, T.; Belanger, D. Electrochem Solid State Lett 2006, 82, 599.
27. Rajendra, P.; Munichandriah, K. J Power Sources 2002, 112, 443.
28. Malinauskas, A.; Mahinauskiene, J.; Ramanavicius, A. Nanotechnology 2005, 16, R51.
29. Gupta, V.; Miura, N. Electrochem Solid State Lett 2005, 8, A630.
30. Fusalba, F.; Gouerec, P.; Villers, D.; Belanger, J. Electrochem Soc 2001, 148, A1.
31. Radhakrishnan, S.; Prakash, X. S.; Rao, C. R. K.; Vijayan, M. Electrochem Solid State Lett 2009, 12, A84.
32. Ding, X. B.; Wan, G. X. J Appl Poly Sci 2001, 79, 1847.
33. Jianguo, D.; ChuanLan, He.; Yuxing, P.; Jianhua, W.; Xingping, L.; Pei, Li.; Albert, S. C. C. Synth Met 2003, 139, 295.
34. Rajendra Prasad, K.; Munichandriah, K. J Electrochem Soc 2002, 149, A1393.
35. Shuangxi, X.; Hongwei, Z.; Guoku, Z. Synth Met 2008, 158, 59.
36. Xing, S. X.; Zhao, C.; Jing, S. Y.; Wang, Z. C. Polymer 2006, 47, 2305.
37. Xing, S. X.; Chu, Y.; Sui, X. M.; Wu, Z. S. J Mater Sci 2004, 40, 215.
38. Zhun, L.; Joseph, W.; Donghai, X.; Gang, C. Small 2008, 4, 462.
39. Moon, Y. B.; Smith, P.; Heeger, A. J. Polym Commun 1989, 30, 196.
40. Wu, N. L.; Wang, S. Y.; Han, C. Y.; Wu, D. S.; Shiue, L. R. J Power Sources 2003, 113, 173.
41. Wu, N. L. Mater Chem Phys 2002, 75, 6.
42. Dong, B.; He, B. L.; Xu, C. L.; Li, H. L. Mater Sci Eng B 2007, 143, 7.
43. Sivaraman, P.; Rath, S. K.;Hande V. R. Thakur, A. P.; Pattri, M.; Samui, A. B. Synth Met 2006, 156, 1057.
44. Belanger, D.; Ren, X.; Davey, J.; Uride, F.; Gottesfeld, S. J Electrochem Soc 2000, 147, 2923.
45. Osaka, T.; Liu, X.; Nojima, M.; Momma, T. J Electrochem Soc 1999, 146, 1724.
46. Rajendra, P. K.; Munichandraiah, N. J Electrochem Soc 2002, 149, A1393.
47. Sun, R. K.; Hong, Y. S.; Park, Y. J.; Wu, X.; Kim, K. M.; Lee, Y. G.; Chang, S. H.; Lee, S. J. Solid State Ionics 2004, 175, 759.
48. Ryu, K. S.; Lee, Y.; Han, K. S.; Park, Y. J.; Kang, M. G.; Park, N. G.; Chang, S. H. Solid State Ionics 2004, 175, 765.
49. Ryu, K. S.; Kim, K. M.; Park, Y. J.; Park, N. G.; Kang, M. G.; Chang, S. H. Solid State Ionics 2002, 152–153, 861.
50. Ryu, K. S.; Wu, X.; Lee, Y. G.; Chang, S. H. J Appl Poly Sci 2003, 89, 1300.
51. Ryu, K. S.; Jeong, S. K.; Joo, J.; Kim, K. M. J Phys Chem B 2007, 111, 731.